SHOALING VIBRATION AMPLIFIER WITH FLATTENED TRANSFER FUNCTION AND SUPPRESSED SPURIOUS MODES

Verena Maiwald[1], Michelle Müller [1], Christian Ritz[1], Cosmin Roman[1] and Christofer Hierold [1]
[1]Department of Mechanical and Process Engineering, ETH Zurich, Zurich, Switzerland

ABSTRACT

An in-plane vibration sensor with off-resonant band-pass displacement amplification and a differential capacitive read-out is presented. The minimum mechanical amplification of 16 dB (i.e. a factor of 6.6) within the designed frequency band from 3-13 kHz is independent of pressure in the range of 6.3 to 64 mbar with a less than 10% change. For a flattened transfer-function a pressure close to 30 mbar is preferred in order to damp the mechanical resonance peaks. The device can be used for low power detection of broadband vibration signals e.g. in monitoring of infrastructure such as bridges and pipelines.

INTRODUCTION

Motivation

Acoustic emission and micro-seismic monitoring requires the detection of broadband, weak signals. While highly sensitive capacitive MEMS acoustic emission sensors have been demonstrated e.g. in [1], they are tuned to a single resonance line and are therefore restricted to a small frequency range. Broadening of the spectrum has been achieved by employing two separate oscillators with different resonance frequency as presented in [2]. Another approach to increase sensitivity over a broad frequency range is to employ displacement amplifying compliant levers such as in [3] where static amplification factors of 40 (32 dB) for a sensing bandwidth of 749 Hz have been demonstrated. These static approaches have a flat frequency response, which means that they are also amplifying low frequency environmental noise. Additionally, their amplification factor is restricted by the torsional stiffness of the lever anchor.

In [4] we introduced a zero-power mechanical motion amplifier. This out-of-plane mechanical transducer showed broadband vibration amplification but suffered from parasitic resonances, a non-flat transfer function with multiple resonance peaks and lacked an electrical read-out.

Device Concept

Here, we present a device based on the same coupled mass broadband amplification as shown in [4] featuring a new in-plane geometry. The device was designed such that parasitic modes are shifted out of the bandwidth by optimized spring design. Further, it was integrated with a differential capacitive read-out. In contrast to the amplification mechanisms relying on resonance ([1] and [2]) or leverage [3] this structure amplifies motion by shoaling the incoming vibration wave through a chain of size-decreasing mass-spring resonators. Thus, the amplification mechanism is significantly less dependent on damping compared to high Q resonant sensors, which are susceptible to long settling times, in-use stiction and usually require high power.

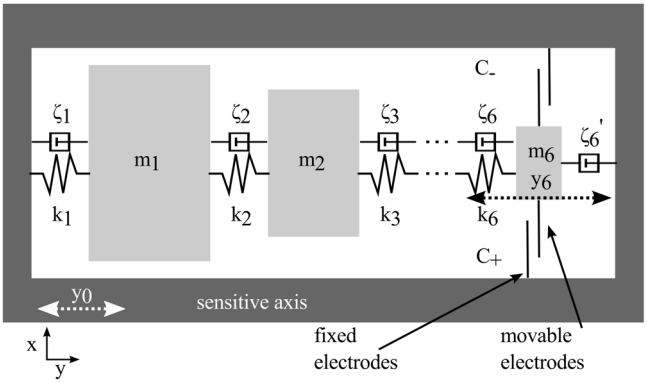

Figure 1: Schematic of the transducer. Six frequency matched masses are coupled in series with decreasing spring constants towards the last mass (m_6). The motion of m_6 relative to the package (y_6) can be read out electrically using the attached differential comb fingers.

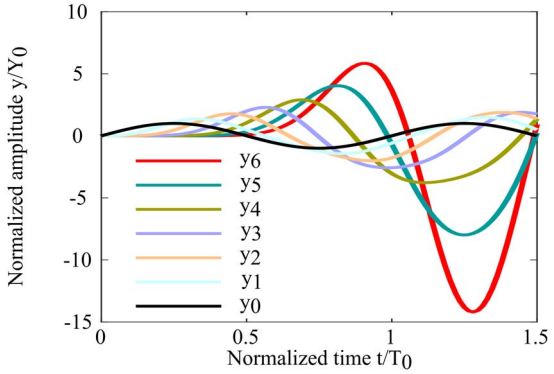

Figure 2: Reduced order model of the off-resonant, time dependent response at 4.65 kHz between the first and second resonance (axes normalized with respect to the input signal amplitude y_0 and period T_0).

The device consists of six matched resonators (angular frequency ω_0) coupled in series of decreasing stiffness (k_i) and masses (m_i) as depicted in Fig.1, according to the design rules:

$$\omega_0^2 = \frac{k_i + k_{i+1}}{m_i} = \cdots = \frac{k_6}{m_6} \qquad (1)$$

and

$$\frac{k_i}{k_{i+1}} = 2 \qquad (2)$$

As a vibration wave reaches the package (y_0), it propagates from m_1 to m_6. Due to the decreasing stiffness k_i and inertia m_i, the wave is shoaled, i.e. the motion amplitude at each subsequent mass y_i increases. Fig. 2 shows a transient simulation of the off-resonant response excited from the rest

position by a sinewave with a frequency of 4.65 kHz. The resulting displacement is the largest for the last mass m_6. Finally, m_6 is equipped with a differential capacitive transducer which can be read out electrically.

METHODS

Finite Element Analysis (FEA)

The design and location of the springs was iteratively adjusted via FEA until parasitic out-of-plane and gimbal modes were shifted outside the device's bandwidth. The mode shapes and Eigenvectors were simulated using the built-in Eigenfrequency study of COMSOL Multiphysics. The anisotropic elasticity matrix for <100> Si with the <110> planes aligned to the x and y axis was used (compare to e.g. [5]). The transfer function presented in the results section was obtained by a frequency domain study excluding damping effects. Both mask undercut of the ICP-DRIE dry etching process as well as the influence of stress were included in the simulation. FEA was also used to simulate the differential capacitive change of the comb-drives including fringe fields by solving the electro statics of the system for a displacement sweep of the last mass (m_6).

Fabrication

The devices were fabricated in a single mask SOI process on 20 µm thick <100> device layer and 4 µm thick sacrificial oxide (see Fig. 3 a). First a 500 nm thick LPCVD deposited SiO_2 mask was patterned using direct laser writing (DLW) of a Photoresist mask and RIE (Oxford NGP 80) dry etching. Then the vertical trenches were etched into the device layer by ICP-DRIE dry etching with a LF 2 step Bosch process (Oxford Estrelas) (Fig. 3 b). After the dry etch the wafer was separated into dies of 3600 µm x 2600 µm with a dicing saw. Subsequently, the movable structures were released using Vapor HF dry etching (SPTS Primaxx, see Fig. 3 c). As adhesion layer for the Au-wire bonds 4/40 nm of Cr/Au was evaporated on top of the structure (Fig. 3 d). Finally, the devices were die- and wire-bonded to a ceramic package using an Au ball-bonder. A released and packaged device is shown in Fig. 4 and Fig. 5.

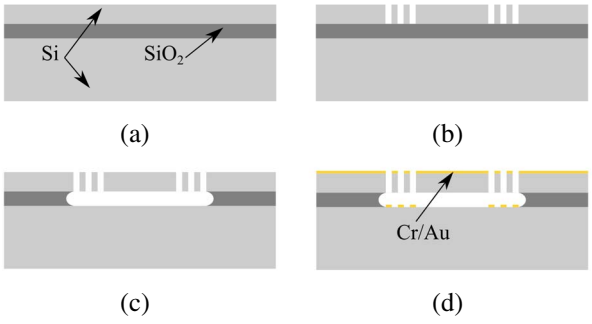

Figure 3: a) The masses were fabricated in a one mask SOI based release process. b) ICP dry etch c) HF vapor dry release d) evaporation of Cr/Au 4/40 nm for electrical contacts

Design

The realized design consists of concentrically arranged proof masses with the largest mass outside and the smallest mass and the bond-pads in the center. The mechanical amplifier is symmetric in x- and y- direction (Fig. 4) and the capacitive comb-drives were designed to enable a differential read-out. Beam type and o-springs were used to achieve preferential movement in the y-direction (Fig. 5). The size of the device was an area of 1642 µm x 2222 µm times the device layer thickness of 20 µm. The separation of the comb-fingers of the capacitive read-out is 1.9 µm.

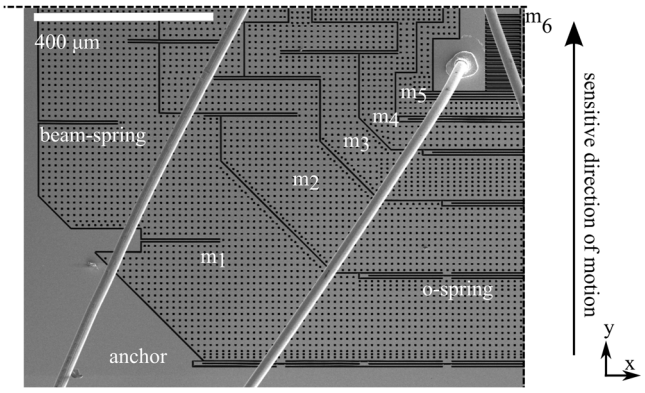

Figure 4: SEM image of one quarter of the fabricated device. The masses are concentrically arranged with the largest mass m_1 on the outside and the smallest mass m_6 in the center. The mechanical amplifier is symmetric along the x and y-axis. Beam and o-springs provide sensitivity in the y direction.

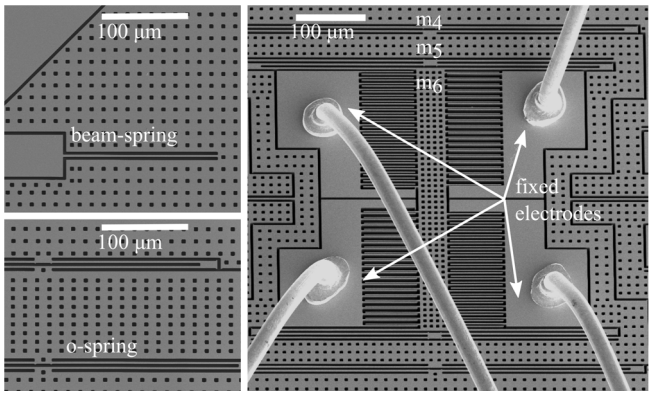

Figure 5: Enlarged view of the springs (left) and the center mass m_6 (right). Au-wire bonds provide connection to the differential fixed electrodes at the center of the device.

Characterization Setup

The capacitive measurement was conducted on a wire-bonded and packaged device. The ceramic package on a PCB was flip-mounted on an in-plane PZT actuator and placed inside a vacuum chamber with pressure control, electrical

feedthroughs and a see through glass window for providing an optical path for characterization. The device was actuated mechanically by a white-noise Voltage signal on the PZT. In order to account for acoustic attenuation of the mounting of the device, the spectrum of the package input displacement y_0 was measured in-situ using a Polytec MSA 400 Laser Doppler Vibrometer (LDV). The capacitive spectrum was acquired using amplitude modulation at 95 kHz and the built-in quadrature demodulation of a Lock-In amplifier (Zurich Instruments).

RESULTS

The transfer function of the device was measured at different pressure set-points between 6.3 mbar and ambient pressure and compared to simulation.

Capacitive Measurement

The capacitive transfer function for a measurement conducted at 6.3 mbar is displayed in Fig. 6. The bandwidth and peak positions agree with the Finite Element Analysis based simulation. The measured transfer function matches the simulated ones with only a ±90Hz deviation of the position of the peaks or maximum 2.5% resonance frequency accuracy. Both mask undercut of the dry etch as well as stress were included in the FEA. At frequencies higher than the mechanical roll-off the signal is not dropping completely which can be explained by the cubic nonlinearity of the read out. From the measured transfer-function the minimum and mean amplification as well as the bandwidth of the amplifier

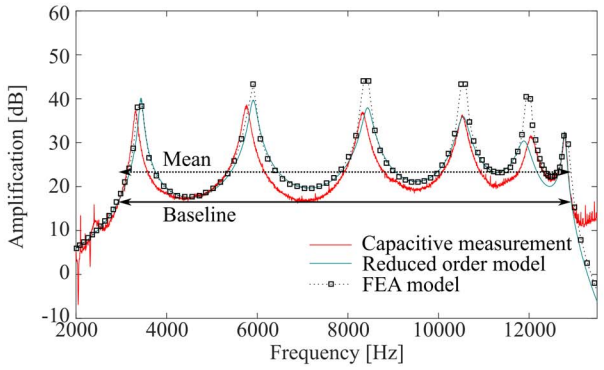

Figure 6: Capacitive measurement vs. model. The position and amplitude of the peaks are in good agreement with the model (±90 Hz). The amplification between 3 kHz-13 kHz is a minimum of 16.4 dB (solid arrow) and a mean of 23.5 dB (dashed arrow). The measurement was conducted at a pressure of 6.3 mbar. The deviation at high frequencies can be explained by the cubic non-linearity of the read-out capacitance.

were extracted. The minimum amplification g_{min} = 16.4 dB is defined as the minimum output between the first resonance (3.32 kHz) and the sixth resonance (12.79 kHz). The amplification bandwidth is the frequency range over which this minimum amplification is achieved. For this device the bandwidth was measured to be 10 kHz over a range from 3-13 kHz). Finally, the mean amplification g_{mean} = 23.5 dB is defined as the mean over said bandwidth. The characteristic frequency f_0 = 7.94 kHz is defined as the center-frequency of the bandwidth.

Reduced Order Model

Two damping coefficients of the lumped model of the system, the perimeter proportional intra-mass damping and the additional damping from the comb-drive were fitted to the experimental quality factors to obtain the damping matrix. The resulting pressure dependent model based on these parameters reproduces well the shape of the measured resonance peaks as can be seen in Fig. 6 (blue line).

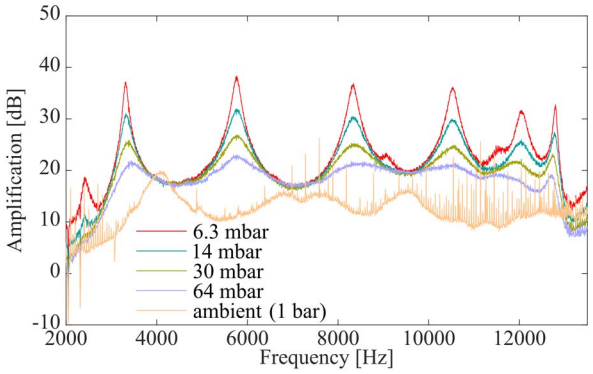

Figure 7: Pressure dependence of the transfer function from 6.3 to 64 mbar and ambient. The baseline amplification deteriorates first for higher pressures between the fifth and the sixth mode.

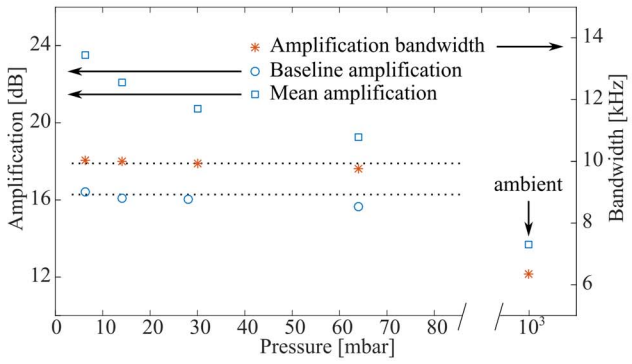

Figure 8: Baseline amplification and bandwidth of the device showed a decrease of less than 10% for a wide pressure range between 6.3 and 64 mbar. The mean amplification is sensitive to the peak amplitudes and therefore to an increase in damping. At ambient pressure the device performance decreases.

Damping and Pressure Dependence

The operational range was identified by measuring at five different pressure set-points between 6.3 mbar and ambient pressure. The peak amplitudes (quality factors)

decrease significantly with increasing pressure (see Fig. 7 and Fig. 8) while the baseline is only reduced by less than 10% up to a pressure of 64 mbar. The baseline starts to deteriorate first at high pressures between the 5th and the 6th mode. At ambient pressure the motion of m_6 is strongly suppressed due to the squeeze film between the comb fingers of the last mass and the readout. Minimum- and mean amplification as well as bandwidth have been extracted for all pressure values and are displayed in Fig. 8.

DISCUSSION

Influence of the Read-out Capacitance on Damping

The integration of a differential capacitance on the last mass enables an electrical read-out of the amplified mechanical signal. At the same time the squeeze film between the comb-fingers (gap 1.9 µm, height 20 µm and length 78 µm) causes additional air damping between the last mass m_6 and the anchor. This air damping influences the resonant response of the device. Understanding the effect of the damping on the system is crucial for identifying the appropriate operating pressure. On the one hand, high quality factors at low pressures yield high motional amplitudes and improve the performance in resonant accelerometers such as [6]. However, they also cause a large dynamic range in the frequency domain and non-linear effects of the capacitive read-out. Together with the signal overshoot and long settling times inherent to underdamped devices, this makes input signal recovery difficult and increases the likelihood of in-use stiction. On the other hand, high pressures (e.g. ambient), which are usually the operating condition for quasi-static accelerometers result in a deteriorated transfer function for this device. Mid-vacuum levels (1.3-13 mbar) have been used for example in packaging of capacitive accelerometers with small sub-µm gaps for co-integration with high frequency gyroscopes [7]. Our measurements show that the low vacuum is also the preferred operating regime for this coupled mass shoaling vibration amplifier.

While a reduction of the peak amplitudes and thereby of the mean amplification is expected with increasing pressure, our data shows that in the transition regime between 6.3 and 64 mbar, the minimum amplification over the complete bandwidth is affected by only -10%. There, a quasi-plateau frequency response can be achieved without sacrificing on the minimum amplification. Also, the low sensitivity of the minimum amplification towards pressure changes relaxes the constraints of achieving and maintaining vacuum in the package. Therefore, the device is preferably operated in this pressure regime around 30 mbar.

CONCLUSION

This work demonstrates a broadband (3-13 kHz) vibration amplifier with improved transfer function. Depending on the pressure in the setup or package, the transfer function is flattened with a minimum amplification of 16 dB almost independently of pressure. We show that damping is an effective way to flatten the transfer function. The transfer characteristic at different pressure set-points between 6.3 mbar and ambient pressure was measured. The FEA and a reduced order model using a damping matrix based on a perimeter proportional squeeze-film damping was compared to the measurement and found to be in good agreement. The peak amplitudes decrease significantly with increasing pressure while the baseline is only reduced by less than 10% up to a pressure of 64 mbar.

ACKNOWLEDGEMENTS

The authors would like to thank the ETH FIRST-CLA and BRNC clean room staff (especially Donat Scheiwiller and Ute Drechsler) as well as Martin Lanz from the Department of Electrical Engineering for their continuous support with fabrication. This research was scientifically evaluated by the Swiss National Science Foundation (SNSF), financed by the Swiss Confederation and funded by Nano-Tera.ch.

REFERENCES

[1] H. Saboonchi and D. Ozevin, “MEMS acoustic emission transducers designed with high aspect ratio geometry,” Smart Materials and Structures, vol. 22, no. 9, p. 095006, 2013.

[2] A. Sorger et al., “Design, modeling, fabrication and characterization of a MEMS acceleration sensor for acoustic emission testing,” in 2013 Transducers and Eurosensors, Barcelona, 2013, pp. 7 26–729.

[3] I. Zeimpekis, I. Sari and M. Kraft, “Characterization of a Mechanical Motion Amplifier Applied to a MEMS Accelerometer,” Journal of Microelectromechanical Systems, vol. 21, no. 5, pp. 1032–1042, Oct 2012.

[4] M. Müller, V. Maiwald, M. Käch, C. Hierold and C. Roman, "A passive micromechanical broadband amplifier for acoustic emission sensing," in 2015 Transducers, Anchorage, 2015, pp. 1129-1132.

[5] M. A. Hopcroft, W. D. Nix, and T. W. Kenny, “What is the Young’s modulus of silicon?” Journal of Microelectromechanical Systems, vol. 19, no. 2, pp. 229–238, 2010.

[6] S. A. Zotov, B. R. Simon, A. A. Trusov and A. M. Shkel, "High Quality Factor Resonant MEMS Accelerometer With Continuous Thermal Compensation," in IEEE Sensors Journal, vol. 15, no. 9, pp. 5045-5052, Sept. 2015.

[7] D. E. Serrano, Y. Jeong, V. Keesara, W. K. Sung and F. Ayazi, "Single proof-mass tri-axial pendulum accelerometers operating in vacuum," 2014 IEEE 27th International Conference on Micro Electro Mechanical Systems (MEMS), San Francisco, CA, 2014, pp. 28-31.

CONTACT

*V. Maiwald, phone: +41-44-6323582;
verena.maiwald@micro.mavt.ethz.ch